Interpack 2005-73073

THERMAL PERFORMANCE OF NATURAL GRAPHITE HEAT SPREADERS

Martin Smalc
Advanced Energy Technology Inc.
A GrafTech International Ltd. Co.

Gary Shives
Advanced Energy Technology Inc.
A GrafTech International Ltd. Co.

Gary Chen
Advanced Energy Technology Inc.
A GrafTech International Ltd. Co.

Shrishail Guggari
Advanced Energy Technology Inc.
A GrafTech International Ltd. Co.

Julian Norley
Advanced Energy Technology Inc.
A GrafTech International Ltd. Co.

R. Andy Reynolds III
Advanced Energy Technologies Inc.
A GrafTech International Ltd. Co.

ABSTRACT

Heat spreaders can be made from natural graphite sheet materials. These spreaders take advantage of the anisotropic thermal properties of natural graphite. Natural graphite exhibits a high thermal conductivity in the plane of the sheet combined with a much lower thermal conductivity through the thickness of the sheet. As a result, a natural graphite sheet can function as both a heat spreader and an insulator and can be used to eliminate localized hot spots in electronic components. In some cases, a natural graphite heat spreader can replace a conventional thermal management system consisting of a heat sink and cooling fan. This paper examines the properties of natural graphite heat spreaders and the application of these spreaders to thermal management problems in laptop computers. The thermal and mechanical properties of natural graphite heat spreaders are presented along with a discussion of how those properties are measured. The use of a natural graphite heat spreader to reduce the touch temperature in a laptop computer is presented. Both experimental techniques and numerical models are used to examine performance of the heat spreader in this application.

KEYWORDS: heat spreader, graphite, anisotropy, and laptop computer

NOMENCLATURE

k_i = in-plane thermal conductivity; W/mK
k_t = thru-thickness thermal conductivity; W/mK
r'_c = specific contact resistance; cm^2-°C/W
r'_j = specific joint resistance; cm^2-°C/W
ΔT_j = temperature rise relative to ambient; °C
t = thickness; mm
L = separation of the two points of temperature measurement in the Angstrom method; cm
Δt = the time difference for the heat to propagate between two points in the Angstrom method; sec
T_1, T_2 = amplitudes of the temperature wave at two points in the Angstrom method; °C
ρ = density; gm/cm^3,
c = specific heat, cal/gm/°C;
m_b = resistance to bending; gm-cm

INTRODUCTION

Heat Spreaders

Various methods of spreading heat are widely used in today's electronics. Heat spreaders are used in die level packaging to spread heat from the microprocessor chip into the packaging. Multi-chip modules have been built that incorporate a copper heat spreader. On a component level, active spreaders such as heat pipes are used to move heat from chip packages to heat sinks. Heat sinks themselves can incorporate spreaders such as a copper base or heat pipes embedded in an aluminum base. Passive heat spreaders have been incorporated into plasma display panels. Spreaders are commonly used within electronic enclosures to move heat from discrete components to the walls of the enclosure.

This paper describes the use of a flexible heat spreader, made from natural graphite sheet, to lower the touch temperature of a laptop computer. This is accomplished by spreading heat from the source, a hard disk drive. The thermal and mechanical properties of the natural graphite heat spreader are presented along with a discussion of how those properties are measured. Experimental techniques and computational fluid dynamic (CFD) models are used to examine performance of the heat spreader in this application. The effect of two major variables, in-plane thermal conductivity and spreader thickness, on the thermal performance of the spreader are investigated.

Flexible Natural Graphite Materials

Natural graphite flakes are a polycrystalline form of carbon comprised of layer planes containing hexagonal arrays of carbon atoms. These layer planes, referred to as graphene layers, are ordered so as to be substantially parallel to one another. The bonding forces holding the graphene layers together are only weak Van der Waals

forces and hence the layers can be readily separated. Natural graphite flakes can be chemically treated to insert an intercalant ion into the interlayer spacing. The graphene layers can then be exfoliated by thermally vaporizing the intercalant in the graphite lattice. The intercalant within the graphite decomposes and volatilizes, which generates internal pressure between the graphene layers and forces the layers to separate as the intercalant escapes the graphite structure. The particles of intercalated graphite expand 100 or more times their original volume in an accordion-like fashion in the direction perpendicular to the graphene layers. The exfoliated graphite particles are vermiform in appearance, and are commonly referred to as worms. These expanded graphite flakes can then be consolidated together and mechanically formed, without binders, into a cohesive, flexible sheet of graphite material. Typically, continuous rolling operations are used to form the worms in sheets.

As shown in Table 1, natural graphite material is highly anisotropic, with a thermal conductivity ranging from 140-500 W/mK in and along the "a" and "b" axes (parallel to the layer planes) and from 3-10 W/mK along the "c" axis (perpendicular to the planes). By comparison, conventional isotropic materials used for spreading heat, such as 1100 series aluminum and 11000 series copper, have a thermal conductivity of 200 and 387 W/mK in all three directions. Natural graphite has a density ranging from 1.1-1.7 g/cm^3 compared to 2.7 and 8.89 g/cm^3 for aluminum and copper respectively. Also, because of their excellent flexibility, natural graphite materials are able to conform well to surfaces under low contact pressures. This combination of properties makes natural graphite a potential substitute for aluminum and copper materials as heat spreaders. In particular, the highly anistropic thermal conductivity of natural graphite implies that a natural graphite sheet can function as both a heat spreader and an insulator and can be used to eliminate localized hot spots in electronic components.

Table 1
Thermal Properties of Heat Spreader Materials

Property	Direction	Natural Graphite Sheet	Aluminum, 1100 Alloy	Copper, 11000 Alloy
Density (g/cm^3)		1.1-1.7	2.71	8.89
Thermal Conductivity (W/mK)	a, b	140-500	220	388
Thermal Conductivity (W/mK)	c	3-10	220	388
Specific Heat Capacity (J/kgK)		846	904	385

PUBLISHED LITERATURE

Heat Spreaders
There are many references to the use of passive heat spreaders in die and chip level packaging. Spreaders for moving heat from chip level packaging into heat sinks were described by Anschel, et al[1]. The use of a heat spreader embedded into a molded plastic electronic package was described by Mahulikar et al[2]. Chu et al describes a heat spreader for a multi-chip assembly[3]

A variety of advanced materials have been proposed for use as heat spreaders. Jagannadham[4] has examined the use of multilayer diamond heat spreader substrates bonded to silicon chips[4]. Use of polycrystalline diamond as a heat spreader between a chip and a heat sink was described by Hall et al[5]. A composite heat spreader, with carbon fibers dispersed in a carbon or metal matrix, was described by Houle[6]. The performance of two dimensional, composite heat spreaders made from carbon-carbon (C-C) and carbon-silicon carbide (C-SiC) materials were measured by Kowbel et al[7]. The thermal performance of these materials was found to be superior to that of metal alloy spreader materials with similar coefficients of thermal expansion such as copper-tungsten.

Advanced materials have also been used as heat spreaders in electronic assemblies and housings. The use of conformal metallic layers applied to the inside of a molded plastic electronics enclosure is described by Watchko et al[8]. The coating provides both heat dissipation and EMI shielding. Weinstein et al investigated the use of a graphite loaded polymer (GLP) as a material for the housing of cell phone handset[9]. The thermal performance of GLP handsets were compared to those of handsets made with conventional acrylonitrile-butadiene-styrene (ABS) and incorporating aluminum or copper heat spreaders. The use of a carbon/carbon heat spreader in a laptop computer was described by Dilley et al[10]. This heat spreader was used to move heat from laptop motherboard to the back of the LCD display. Carbon fibers in various orientations were used to form heat transfer conduits to move heat from an absorption plate and spread the heat uniformly across the back of the LCD display. Murthy et al studied the performance of two- phase heat spreaders that incorporated microfabricated structures to enhance boiling[11].

Anisotropic Heat Spreaders
The use of natural graphite material as a heat spreader was examined in CFD models by Tzeng et al[12]. In a simplified model, Tzeng showed that an anistropic heat spreader, with properties similar to those of natural graphite, could lower the maximum temperature of a localized heat source. A heat spreader made from highly ordered pyrolytic graphite was described by Ritchey, III[13]. The pyrolytic graphite had a thermal conductivity in the a and b planes of 1500 W/mK. The use of a similar pyrolitic graphite heat spreader was described by Messenger et al[14]. In this application, the pyrolytic graphite was encapsulated in aluminum and bent into an L shape and was used to transfer heat from an electronics enclosure to an external mounting rack.

Spreading heat and cooling components in laptop computers poses unique problems. Because of the high density of components packed within a laptop, very little room is available for a thermal solution. The design of thermal management system for an ultra-thin laptop was described by Kobayashi et al[15]. Two aluminum heat spreaders, one coupled to a lower case made of die cast magnesium alloy, the other to an upper case of ABS plastic, were used to cool a 3.9W Pentium processor by natural convection only. Thermally conductive silicon gap pads were used to conduct heat from the microprocessor and motherboard to the rigid aluminum heat spreaders. One disadvantage of this design is that the case temperature immediately below the heat source can be high. In later work, Kobayashi et al, described the replacement of the rigid aluminum spreaders with flexible graphite heat spreaders[16]. Thermally insulating elastomeric materials were placed between the graphite and the case and were used to press the graphite against the heat source. The anisotropy of the graphite, combined with the insulation of the elastomer, eliminated the hot on the case beneath the heat source.

HEAT SPREADING IN LAPTOP COMPUTERS

Temperature Distribution In a Typical Laptop Computer

A typical, medium performance, laptop computer is shown in Fig. 1, while Fig. 2 shows the internal layout of components directly below the keyboard and case. Major components include the heat sink, the heat pipe above the CPU chip, the fan, the slot for the PCMIA card, the hard drive, the battery, and the bay for the DVD drive. There is a well-designed thermal solution cooling the CPU, but there is no explicit thermal solution employed to cool the hard drive. Because of economic factors, standardization is widespread and the layout of this unit is typical of many laptops. A particular feature of this design is the placement of the hard drive under the left palm rest and the battery under the right. High hard drive operating temperatures can result in uncomfortable palm rest touch temperatures.

Fig. 1: Typical laptop computer used in tests
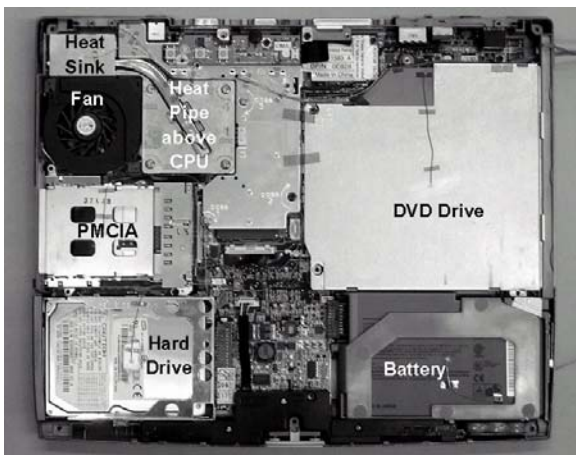
Fig. 2: Internal components located immediately under the case and keyboard

To determine maximum hard drive temperature, an AVI file, loaded onto the hard drive, was run continuously for 2 hours and on-board software was used to access a temperature sensor built into the hard drive. An infrared thermal image of the laptop case taken at the end of this period is shown in Fig. 3. The image was made with an Infra-Red Solutions Inc., Flex Cam model FLX-031115. To provide for accurate temperature readings, the cover of the laptop was coated with flat black paint. Four areas of the image were highlighted and the average temperatures within those areas were determined using Flex View V1.0.16 Image Analysis Software. Area A1 is the area of the left palm rest, A2 the mouse pad, A3 the right palm rest, and A4 an area on a flat black, insulating surface adjacent to the laptop that was used to obtain an ambient temperature measurement. The average temperature in each area was determined and the average temperature rise relative to ambient, ΔT_{avg}, determined. These results are shown in Table 2, along with the increase in hard drive temperature from the internal sensor.
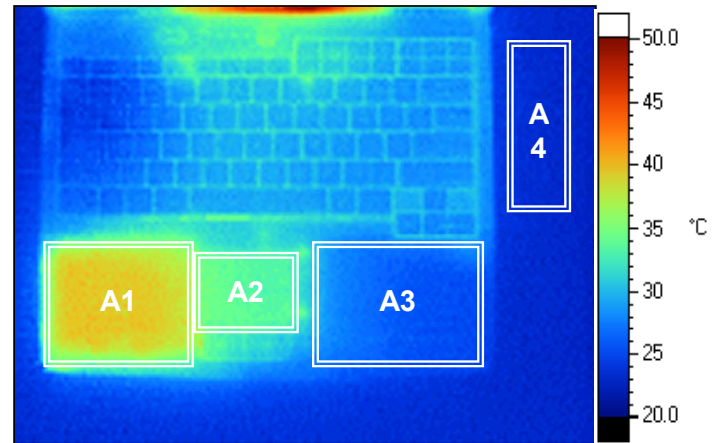
Fig. 3. Thermal image of the laptop cover and keyboard taken after running an AVI file continuously for 2 hours

Table 2 Hard Drive and Laptop Case Temperature				
Average Temperature Rise Above Ambient (°C)				A4 Ambient (°C)
Hard Drive	A1 Left Palm Rest	A2 Mouse Pad	A3 Right Palm Rest	
30.0	14.1	9.9	3.0	23.9

As shown, the on-board monitoring program indicated that the hard drive reached a temperature of 30°C above ambient. This is similar to data obtained by Vichare et al, who reported that in an in-situ study of laptop operating temperatures, hard drive temperatures of 25-30 °C above ambient occurred ~30% of the time[19]. This increase in hard drive temperature caused the average temperature of the left palm rest to increase to 14.1 °C above ambient while that of the right palm rest has increased only 3.0 °C. This increase in left palm rest temperature can result in uncomfortable surface touch temperatures for the user. Two references indicate that users of various laptops have complained about high palm rest operating temperatures[17], [18].

This test shows that significant temperature gradients exist in laptop computers. The remainder of this paper will examine how a natural graphite heat spreader can be used to reduce these temperature gradients.

Experimental Design

To determine the effect of graphite spreaders on the heat distribution within the laptop, thermal tests were conducted on the laptop in Fig. 1 with and without spreaders. Although the thermal imaging camera was used to provide basic case temperature data, thermocouples were used for primary measurements of component, spreader, and case temperatures. For the spreader tests, two independent variables were selected for examination; graphite in-plane thermal conductivity, and graphite thickness. Each variable was tested at a low and high level; nominal values chosen for each are shown in the test matrix in Table 3.

Table 3
Graphite Spreader Test Variables

Variable	Level	Nominal Value
Graphite thickness	Low	0.25 mm
	High	0.50 mm
Graphite in-plane thermal conductivity	Low	250 W/mK
	High	380 W/mK

Material Properties

The in-plane thermal conductivity, thru thickness thermal conductivity, specific thermal contact resistance, and resistance to bending are the four most significant material properties that could affect the performance of natural graphite heat spreaders in the laptop application. The in-plane thermal conductivity, k_i, directly effects the ability of natural graphite to spread heat away from a point source, while the thru-thickness thermal conductivity, k_t, affects heat transfer through the material. The specific thermal contact resistance, r_c', influences how well heat is transferred between the spreader and the internal components of the laptop. Finally, the resistance to bending, m_b, shows how easily the spreader can conform to differences in the height of the heat sources and sinks. A brief description of test techniques used to measure each property is given, followed by a summary of the properties of all of the spreader materials tested.

In-plane Thermal Conductivity Testing

The value of k_i was measured using a thermal diffusivity technique, developed by Wagoner et al[20], based on a method invented by Angstrom in 1861. In this technique, the temperature of a long specimen is varied sinusoidally at one end and measurements are taken on the resulting heat wave as it progresses down the specimen. Because of the high degree of anisotropy in natural graphite, this technique is ideally suited to measuring k_i. As shown in Fig. 4, a test specimen is mounted on a specimen holder that is placed in the vacuum chamber. One end of the specimen is affixed to the heat source while the other end is maintained under a light spring tension. Thermocouples TC1 and TC2 contact the specimen at two points some distance away from the heat source and are used to measure the time delay and the amplitude of the temperature wave at these points.
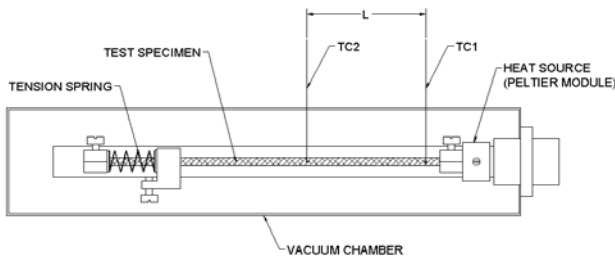
Fig. 4: Schematic of apparatus used to measure the in-plane thermal conductivity using Angstrom's Method

The in-plane thermal conductivity is given by,

$$k_i = \frac{100 \, \rho \, c \, L^2}{2 (\Delta t) \ln\left(\dfrac{T_1}{T_2}\right)} \tag{1}$$

where,
L is the separation of the two thermocouples TC1 and TC2,
Δt is the time difference for the heat to propagate from the first to the second thermocouple,
T_1 and T_2 are the amplitudes of the temperature wave as measured by TC1 and TC2,
ρ is the density of the specimen, and
c is the specific heat.

Tests are carried out in a 0.08 milliTorr vacuum. Test specimens 450 mm long by 3.0 mm wide are extracted from the spreader material. Specimen temperatures are measured using two type E, 0.001inch diameter bare thermocouples. Spring tension of the thermocouple wires holds the thermocouple bead against the surface of the specimen. The heat source is a Peltier type thermoelectric module, Melcor model SH 1.0-23-06L, with a thermal power rating of 4.7 Watts. The Peltier module is powered by a Hewlett Packard HP 3325B Synthesizer/Function Generator operating at 0.016 Hertz. Temperature data is measured using a Hewlett Packard HP 3497 Data Acquisition unit. Tests are conducted at a nominal temperature of 22 °C and the sinusiodal variation in specimen temperature is on the order of +/-1 °C. Six hundred data points are collected and a sinusoidal curve is fitted to the data using a least squares method. Standard deviation of the measured in-plane thermal conductivity of a 233 W/mK standard is 6.3 W/mK or 2.7 %.

Formula (1) requires the determination of the specific heat of the natural graphite materials. Specific heat was determined using differential scanning calorimetry per ASTM Standard E1269-05[21]. Samples were tested on a TA Instruments 2910 Differential Scanning Calorimeter. The reference standard used was synthetic sapphire. The measured specific heat of all 4 materials was 0.170 cal/gm °C at 25 °C. This is a value that is well established for all forms of natural and artificial graphite[22].

Thru-thickness Thermal Conductivity and Thermal Contact Resistance

The thru-thickness thermal conductivity k_t, and the specific thermal contact resistance, r_c', were measured using a modified version of the test method described in ASTM Standard D5470[23]. This standard describes a technique to determine the thru-thickness thermal conductivity of thin materials by measuring the steady state heat flux through a flat specimen. This test method has been previously used by Smalc et al[24] to determine k_t and r_c' for graphite thermal interface materials. The same equipment and techniques were used to measure these properties in the spreader materials. A brief summary of the method is given below.

In these tests, a specimen is sandwiched between a pair of aluminum meter bars, and a heater and cooling plate are used to generate a one-dimensional heat flow through the specimen. A test pressure of 25 kPa is applied to the meter bars to simulate a contact pressure typical of electronic applications. Thermocouples located in each meter bar are used to measure the thermal gradient in each bar. From these thermal gradients, the surface temperature of the specimen is determined. Knowing the thermal conductivity of the meter bars, the heat flow through the specimen is determined and from this, the specific thermal joint resistance, r_j', of the specimen can be

determined. The specific joint resistance, r_j', is the thermal resistance of the entire joint between the meter bars and includes both the specific contact resistance, r_c', and the specific thermal resistance resulting from the thru-thickness thermal conductivity of the specimen.

To determine k_t for a given spreader material, measurements of r_j' are made on three different thicknesses of the material, by stacking up individual specimens. The specific joint resistance is then plotted as a function of specimen thickness. A straight line is fitted to the points using a least squares technique and the thermal conductivity is given by the inverse of the slope of this line. The specific contact resistance of spreader material, r_c', with the aluminum meter bar surfaces is given by the y-intercept of this line. Although specific contact resistance varies with the surfaces used in the actual application, this test method provides a standardized number that can be used to compare the performance of different materials.

It is assumed that under pressure, the individual graphite specimens in the stack coalesce together and that any contact or gap resistance between the specimens is negligible. This assumption is reasonable based on the layered structure of natural graphite. Tests have shown that for a typical natural graphite material, the standard deviation in the measured value of k_t is 14 %, while the standard deviation in measured value of r_c' is 9%.

Natural graphite is an electrical conductor with a typical in-plane electrical resistivity of 6.8 $\mu\Omega$m[25]. Since the natural graphite spreader contacts components of the laptop that may be electrically charged, an electrically insulating sheet of polyester (PET) film was affixed to the spreader to prevent shorting. PET materials are commonly used as low cost electrical insulators in electronic applications. The thickness of a PET insulating film can vary from as little as 2.5 μm to 0.36 mm. The 2.5 μm has a dielectric breakdown voltage of 490V and is used in capacitors[26]. As the thickness increases, both the dielectric breakdown voltage and the thermal resistance of the material also increase. PET films are available in roll form and can economically be applied to natural graphite materials in a continuous process. Where low thermal resistance is critical, such as in thermal interface materials, 2.5 μm PET films have been attached to natural graphite to provide electrical insulation. These thin films tend to be costly and are not practical for large spreaders where thicker, more durable films are required. For the spreaders used in these tests, a 13 μm thick PET film was chosen and attached to the top and bottom of the graphite spreader using a thin layer of acrylic adhesive.

This PET layer greatly increased the specific contact resistance of the graphite spreader. To determine this effect, a modification was made in the 3 specimen stacking test. In the first test, a sample of graphite spreader material was tested that had the PET layer applied to both the top and bottom surfaces. In the second test, two graphite samples were tested; the bottom sample had the PET layer applied to its bottom surface and the top sample had the PET layer applied to its top surface; contact between the two samples was through the exposed graphite surfaces. In the third test, an uncoated graphite spreader was sandwiched between the two specimen used in the second test. This procedure ensured that in all tests, a 13 μm PET layer contacted the meter bars and that contact between specimens was through uncoated graphite layers. Thus, the contact resistance that was measured resulted primarily from the PET surface layer and is the same for all four spreader materials.

Resistance to Bending

The resistance to bending, m_b, was measured using the test method described in ASTM D5342[27]. This method describes a test technique to determine the bending moment required to deflect the free end of a 38 mm wide, vertically clamped specimen, 15 ° from its center line, when the load is applied 50 mm away from the clamp. The instrument used is designed to measure variations in the bending moment, m_b, from 1 g-cm to 10,000 g-cm. The technique has a repeatability of 9-20% in the 0 to 100 g-cm range and 10% in the 1 to 500 g-cm range.

In this test, the specimen undergoes simple cantilever bending. For conventional materials such as aluminum and copper, the resistance to bending can be calculated based on specimen dimensions and modulus of elasticity. This technique has been found to be very useful in testing natural graphite materials where bending resistance cannot be easily calculated. Natural graphite sheets are produced in a rolling operation, and tests have not shown any differences in thermal properties between the rolling direction and the direction 90 ° to the rolling direction. However, there are differences in the resistance to bending in these two directions. Additionally, the presence of a PET surface layer also affects m_b. To account for this, specimens from each spreader were tested in the both the rolling direction and across the rolling direction. Samples of 1100 aluminum alloy and 11000 copper alloy were also tested for comparison.

Properties of the Materials Tested

The measured properties of the graphite spreader materials, actually tested in the laptop, are shown in Table 4. The four different spreader materials were prepared individually and there were some variations in the values of the test variables that were proposed in Table 3. In general, the low values of thickness are within 4-8% of the nominal value, while the high values are within 2-4 % of the nominal. The low values of k_i are within 6-10% of the nominal, while the high values are within 3% of the nominal.

Table 4
Properties of Graphite Spreader Materials used in Laptop Testing

Test Variable		Graphite Thickness (mm)	k_i Graphite Only		k_t Graphite Only (W/m°K)	r'_c Graphite per side cm²-°K/W	r'_c PET Film per side cm²-°K/W	Resistance to Bending	
Thickness	k_i		Mean (W/m°K)	Standard Deviation (W/m°K)				Rolling Direction (gm-cm)	90° to Rolling Direction (gm-cm)
Low	Low	0.27	234	9	4.51	0.22	1.57	34	28
High	Low	0.52	275	8	4.94	0.15	1.57	143.	110
Low	High	0.26	393	13	3.81	0.51	1.57	51	40
High	High	0.51	369	14	3.33	0.32	1.57	290	187

Properties of aluminum 1100 alloy and copper 11000 alloy materials are shown in Table 5. Note the high resistance to bending of the aluminum and copper sheets compared to that of the graphite materials. The graphite materials have a resistance to bending that is generally less than that of aluminum alloys that are half their thickness. The 0.38 mm copper sheet, with a thermal conductivity in the same range as that of the in-plane thermal conductivity of the best graphite material, has a resistance to bending that is more than 5 times higher than that of the graphite. Clearly the graphite materials are considerably easier to bend than the aluminum and copper materials.

Table 5
Comparative Properties of other Materials

Material	Thickness (mm)	k_i (W/mK)	k_t (W/mK)	r_c (per side) cm²-K/W	Resistance to Bending (gm-cm)
Aluminum 1100 alloy	0.13	220	220	-	5
Aluminum 1100 alloy	0.25	220	220	-	304
Copper 11000 alloy	0.38	388	388	-	1563

APPLICATION OF A GRAPHITE HEAT SPREADER TO THE LAPTOP

Experimental Methods

The natural graphite material used in these tests was eGraf® SpreaderShield™ provided by GrafTech Inc., of Cleveland, Ohio. The overall dimensions of the graphite spreader used in these tests are shown in Fig. 5. Overall dimensions of the spreader are 231 mm x 300 mm. The spreader was designed to contact the hard drive and all components cooler than the hard drive. This was done by analyzing a thermal image of the cover of the computer, Fig. 3, and carefully mapping out those areas cooler than the area immediately over the hard drive; the assumption being that the temperature gradient in the cover reflects the underlying gradient in the components. The keyboard is built with raised plastic keys and switches affixed to an aluminum plate. Because the keys are raised up, they are cooler than the plate. Plate temperatures, however, are visible in the spaces between the keys and these were used for the thermal map. The perimeter of the spreader was then modified to account for the detailed shape of the case, and various slots were added to account for mounting screws, etc.
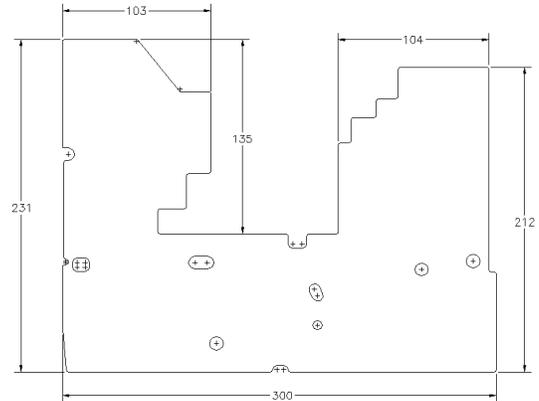
Fig. 5. Overall dimension of the natural graphite spreader

The spreader is designed to lie on top of the components and held in place by the contact pressure generated by the case. Because the surfaces of the components are at different heights, the spreader undergoes considerable deformation at installation. Fig. 6a shows a 0.52 mm thick graphite spreader as it is being installed in the laptop and Fig. 6b shows this spreader after testing. Note the visible deformation in the spreader, particularly in the areas over the hard drive and battery. The graphite spreaders were not formed to shape prior to installation in the laptop; deformation of the spreaders occurred when the laptop was reassembled. No difficulty was encountered in reassembling the laptop with the spreaders in place.
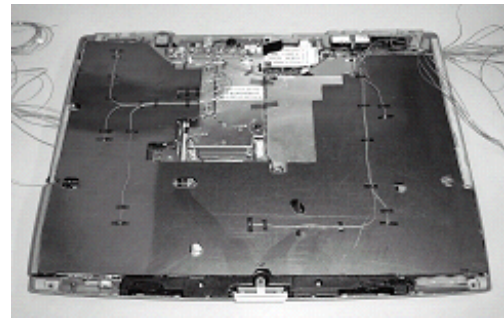
Fig. 6a. The 0.52 mm thick, 275 W/mK natural graphite spreader being installed in the laptop.
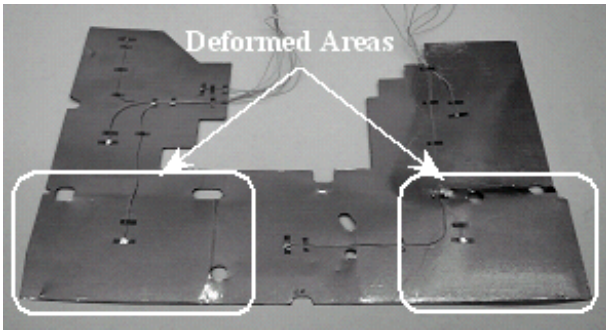
Fig. 6b. The same spreader showing significant deformation after testing

Thermocouples were affixed to the centers of the heat sink, the heat pipe directly above the CPU, the PMCIA slot, the hard drive, the battery, and the DVD drive. Two corresponding sets of thermocouples were affixed to the top and bottom surfaces of each spreader, directly above those on the components. Finally, a fourth set of thermocouples was affixed to the top of the case and the bottom of the aluminum keyboard mounting plate, in locations corresponding to those on the components. An additional set of thermocouples was mounted on the mouse pad and on the top and bottom surfaces of the spreader directly under the mouse pad. With this arrangement, temperatures can be mapped horizontally on the components and vertically from the components through the spreader and to the case. An additional thermocouple was used to measure ambient temperature.

Type T, 0.13 mm diameter thermocouples used were and the thermocouple beads were affixed with an alpha cyanoacrylate adhesive. A small drop of thermal paste was placed on each bead and the bead was then covered with Kapton tape. An Agilent 34907A Data Acquisition Switch unit equipped with two Agilent 34901A 20 Channel Mulitplexer cards was used to measure thermocouple temperatures. In addition, on-board software was used to read the temperature sensors built into the hard drive and the CPU chip. Throughout all the tests, the on-board hard drive sensor measured a temperature 3-4 °C higher than the temperature measured by the thermocouple on the outside of the hard drive, while the temperature measured by the on-board sensor on the CPU chip was within 0-1 °C of that measured by the thermocouple on the heat pipe above the chip. Repeated testing showed that for average thermocouple temperatures between 20-50 °C, the standard deviation was 0.4 °C or about 1%.

All tests were conducted in a laboratory area where air currents were kept to a minimum. Ambient temperature was maintained between 22.0–23.1 °C during the course of all the tests. The laptop base was insulated by placing it on an insulating material. An AVI file, stored on the hard drive, was run continuously for 120 minutes to heat up the drive; thermal stability was reached after 100 minutes. Test data was recorded at 30-second intervals over the last 10 minutes of testing and averaged. Supplemental thermal data on case temperatures was provided using the thermal imaging system described previously.

Experimental Results

The temperature rise relative to ambient, ΔT_i, at each thermocouple location, was computed for each test condition. The temperature rise at the hardware level, for all test conditions, is shown in Table 6 and Fig. 7.

			Table 6		
		Temperature Rise of Hardware Components			
Spreader Material	None	0.27 mm 234 W/mK	0.52 mm 275 W/mK	0.26 mm 393 W/mK	0.51 mm 369 W/mK
Location	ΔT_i (°C)	ΔT_i (°C)	ΔT_i (°C)	ΔT_i (°C)	ΔT_i (°C)
Heat Sink	9.0	10.5	10.4	10.4	10.3
CPU	9.6	11.0	10.9	10.9	10.8
PMCIA Slot	7.3	11.5	13.0	11.2	11.6
Hard Drive	27.8	23.8	22.8	22.6	21.9
Battery	4.8	8.1	9.3	7.8	9.0
DVD Drive	9.9	10.3	10.9	9.8	10.7
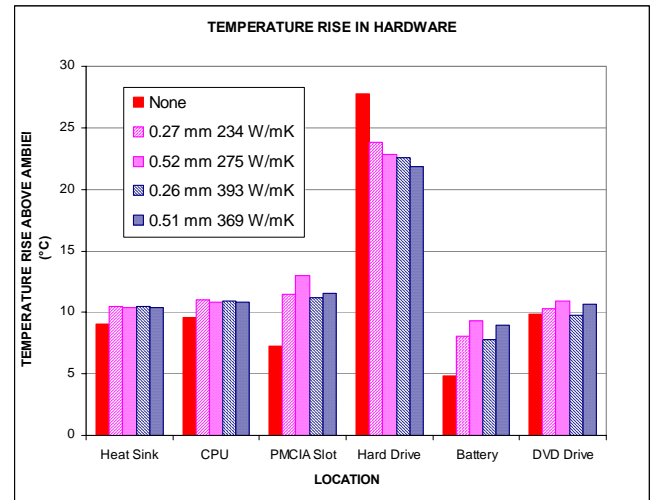
Fig. 7. Temperature rise in the hardware components

As shown, for the baseline condition, the temperature of the hard drive has increased to 27.8 °C above ambient. The use of the spreader material decreases this by as much as 21%, to 21.9 °C for the 0.51 mm 369 W/mK spreader. The data clearly shows that the temperature of the other components increases in the presence of the spreader material. Components nearest to the hard drive, notably the battery and the PMCIA slot both show the largest increase in temperature. The use of the 0.52 mm thick 275 W/mK spreader causes the largest increase in PCMIA and battery temperature, with the PCMIA temperature increasing by 5.7 °C and the battery increasing by 4.5 °C. The heat sink shows an increase in temperature of only 1.3-1.5 °C regardless of the spreader used, and the CPU shows an increase of 1.2-1.4 °C. Clearly the temperature gradient in the hardware components has been altered by the spreaders. The graphite spreaders have transferred heat from the hottest component (the hard drive) into the cooler surrounding components. The data shows that increasing either spreader thickness or in-plane thermal conductivity will improve heat flow and reduce the overall temperature gradient in the components.

The corresponding temperature distributions on the case are shown in Table 7 and Fig. 8. The data shows a baseline temperature rise of 16.2 °C in the left palm rest above the hard drive. This is reduced by 35%, to 10.5 °C using the 0.51 mm 369 W/mK spreader. This spreader also reduced the temperature rise of the mouse pad, adjacent to the hard drive, by 17%, from 10.3 °C to 8.6 °C. The temperature rise of the right palm rest, above the battery, increased from 2.9 °C to 7.3 °C. Thus, the overall gradient in temperature on the case has been reduced.

Table 7
Temperature Rise of External Case

Spreader Material	None	0.27 mm 234 W/mK	0.52 mm 275 W/mK	0.26 mm 393 W/mK	0.51 mm 369 W/mK
Location	ΔT_i (°C)	ΔT_i (°C)	ΔT_i (°C)	ΔT_i (°C)	ΔT_i (°C)
CPU	10.3	9.9	10.3	9.3	9.8
PMCIA Slot	8.9	9.3	9.7	8.8	9.3
Hard Drive Left Palm Rest	16.2	13.1	11.8	11.8	10.5
Mouse Pad	10.3	9.6	9.6	8.6	8.6
Battery Right Palm Rest	2.9	5.8	7.2	5.7	7.3
DVD Drive	8.1	10.9	11.0	10.5	10.6
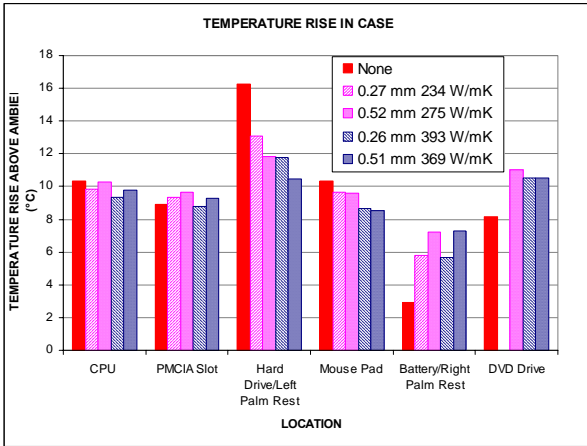
Fig. 8. Temperature rise of the external case

This reduction in case temperature is further confirmed by the thermal image of the laptop with the 0.51 mm 369 W/mK spreader in place shown in Fig. 9. Average temperature data from this image and from Fig. 3 are presented in Table 8 which shows the reduction in the average temperature rise on the surfaces of the laptop. As shown, the difference in the average temperature of the left and right palm rest areas has been reduced from 11.1 °C when no spreader is used to only 2.9 °C with the 0.51 mm 369 W/mK spreader.

Fig. 9. Thermal image of the laptop cover and keyboard taken with the 0.51 mm 369 W/mK graphite spreader in place

Table 8
Thermal Performance of Laptop - Thermal Imaging Data

Spreader	Average Temperature Rise Above Ambient (°C)				A4 Ambient (°C)
	A1 Left Palm Rest	A2 Mouse Pad	A3 Right Palm Rest	ΔT Left to Right Palm Rest	
None	14.1	9.9	3.0	11.1	23.9
0.51 mm 369 W/mK	8.8	7.6	5.9	2.9	23.7

The temperature increases at the bottom of the spreaders are shown in Table 9 and Fig. 10. Notice that in general, these follow the same trends shown in the hardware temperature, which is to be expected. Note that the higher the hardware temperature rise, the greater the difference between the temperature rise in the spreader and the hardware. At the hard drive, the difference between hard drive and bottom spreader temperatures varies from 4.4-5.6 °C, at the heat sink, this difference is only 0.3-0.8 °C and at the DVD drive the difference is 0.5 °C. Clearly these differences reflect the thermal resistance of the interface between the spreader and these components and differences in heat flux at each location.

Table 9
Temperature Rise at Bottom of Spreader

Spreader Material	0.27 mm 234 W/mK	0.52 mm 275 W/mK	0.26 mm 393 W/mK	0.51 mm 369 W/mK
Location	ΔT_i (°C)	ΔT_i (°C)	ΔT_i (°C)	ΔT_i (°C)
Heat Sink	9.7	9.8	9.7	10.0
CPU	11.1	11.1	10.8	11.0
PMCIA Slot	11.6	12.7	11.4	11.7
Hard Drive	18.8	18.4	17.2	16.3
Mouse Pad	15.6	15.0	14.5	13.8
Battery	8.6	10.0	8.6	9.8
DVD Drive	9.8	10.4	9.3	10.2
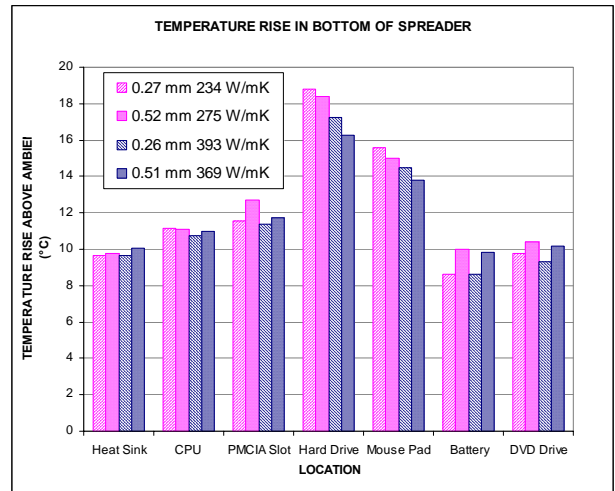
Fig 10. Temperature rise in the bottom of the spreader

The bottom to top temperature gradients within each of the spreaders is shown in Table 10 and Fig. 11. In general, these temperature gradients are small, in many cases less than the standard deviation in

temperature measurement. However, these gradients are largest over the areas of the highest heat flux, namely the hard drive.

Table 10 Δ T Spreader Bottom to Top				
Spreader Material	0.27 mm 234 W/mK	0.52 mm 275 W/mK	0.26 mm 393 W/mK	0.51 mm 369 W/mK
Location	ΔT_i (°C)	ΔT_i (°C)	ΔT_i (°C)	ΔT_i (°C)
Heat Sink	0.3	0.3	0.3	0.4
CPU	0.3	0.3	0.2	0.3
PMCIA Slot	0.3	0.6	0.3	0.1
Hard Drive	0.9	1.6	0.5	1.2
Mouse Pad	0.6	0.7	0.7	0.7
Battery	0.0	0.2	0.1	0.1
DVD Drive	0.1	0.3	0.2	0.3
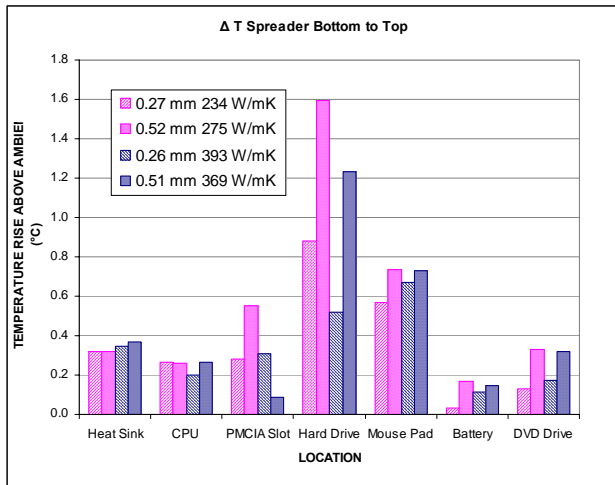
Fig. 11. Bottom to top temperature gradient within the spreader

Numerical Modeling

As shown in Table 4, the contact resistance of a PET coated spreaders is 5-10 times higher than that of a corresponding uncoated spreader. In a thermal interface material, this increase in contact resistance would severely degrade performance. Determining the effect of this increase in contact resistance on a heat spreader is more difficult. Laptop tests on uncoated graphite spreaders cannot be performed because of the problem of electrical shorting. Instead, the effect was studied using CFD modeling.

Using data from these tests, CFD models were constructed for each spreader tested. The CFD software used was IcePak Ver. 4.1 by Fluent Inc. These models were constructed using the contact resistance measured for the PET coated spreaders. Table 11 shows a comparison of the maximum temperature rise measured on the hard drive and predicted by the model. Boundary conditions for the model were adjusted to obtain good agreement between the model and the measurements for all four spreaders. The hard drive power dissipation was unknown and the numerical model was used to estimate it. The model indicates that hard drive is generating 16 watts of heat.

Table 11 Modeling Results - Temperature Rise above Ambient at Hard Drive				
Spreader Material	0.27 mm 234 W/mK	0.52 mm 275 W/mK	0.26 mm 393 W/mK	0.51 mm 369 W/mK
Method	ΔT_i (°C)	ΔT_i (°C)	ΔT_i (°C)	ΔT_i (°C)
Measured	23.8	22.8	22.6	21.9
Modeled	24.1	22.8	22.5	21.9

Temperature distributions computed from the CFD model are shown in Fig. 12a, for the 0.27 mm 234 W/mK spreader, and Fig. 12b for the 0.051 mm 369 W/mK spreader. Note the reduced gradient and the lower temperatures in the 369 W/mK spreader.

(a)

(b)
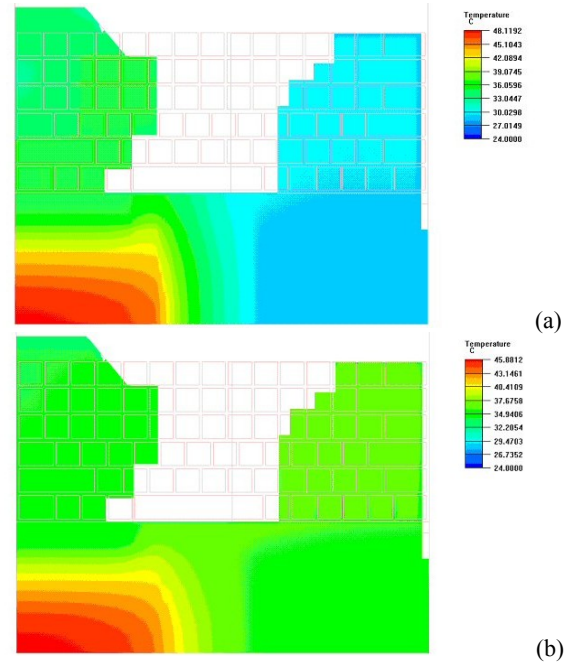
Fig. 12. Spreader temperature distributions from CFD model for a) 0.27 mm 234 W/mK spreader and b) 0.51 mm 369W/mK spreader

These models were used to determine the effect of removing the PET layer from the graphite spreader. Two cases were studied, the 0.52 mm 275 W/mK spreader and the 0.51 mm 369 W/mK spreader. The hard drive wattage was fixed at 16 Watts and the temperature rise above ambient was determined at the hard drive, the battery, the left palm rest above the hard drive and the right palm rest above the battery. Results of these models are shown in Table 12 and 13.

Table 12 Thermal Modeling Results - 0.52 mm 275 W/mK Spreader				
Contact Resistance	Temperature Rise Above Ambient (°C)			
	Hard Drive	Case above Hard Drive	Battery	Case above Battery
1.57	22.81	11.83	6.35	4.47
0.15	22.42	11.66	6.24	4.42
Temperature Increase due to PET (°C)	0.39	0.17	0.11	0.05

Table 13
Thermal Modeling Results - 0.51 mm 369 W/mK Spreader

Contact Resistance	Temperature Rise Above Ambient (°C)			
	Hard Drive	**Case above Hard Drive**	**Battery**	**Case above Battery**
1.57	21.88	11.31	6.96	4.61
0.32	21.86	11.31	6.54	4.40
Temperature Increase due to PET (°C)	0.02	0.01	0.42	0.21

As shown in these tables, removing the PET layers will reduce all these component and case temperatures. The PET layers contribute to a maximum increase in component temperature of about 0.4 °C and a maximum increase in case touch temperature of about 0.2 °C. For the lower thermal conductivity spreader, the maximum temperature increase occurs in the hard drive area while for the higher thermal conductivity spreader, this maximum temperature increase occurs in the battery area.

The 0.52 mm 275 W/mK spreader with PET reduced the hard drive temperature by 5.0 °C, and the removal of the PET layer would improve this by only about 8%. This spreader with PET reduced the palm rest temperature above the hard drive by 4.4 °C; the removal of the PET layer would improve this by only about 4%. The reason for the relatively minor effect of the PET contact resistance appears to be that the thermal power passing through the spreader is relatively low and there is no single highly concentrated heat source. Heat transfer in and out of the spreader occurs over a relatively wide area. For practical purposes, these increases in temperature due to the PET layer are negligible compared to the overall changes in temperature achieved by the spreaders.

CONCLUSION

The thermal and mechanical properties of natural graphite heat spreaders have been presented. The use of these spreaders to cool a hard drive in a typical laptop computer has been described. Test results have been presented for spreaders made with materials at two different thicknesses and with two different in-plane thermal conductivities. The effect of thickness and in-plane thermal conductivity on cooling the hard drive has been examined. Results presented showed that best performance was obtained from a 0.51 mm thick natural graphite spreader that had an in-plane thermal conductivity of 369 W/mK. Installed in a laptop, the natural graphite spreader was able to conform easily to the height differences of the components it contacted. The data shows that this spreader reduced the overall temperature gradient within the laptop and on the outer case. Heat was transferred from the hard drive, which generated an estimated 16 watts of heat, to other areas of the laptop and reduced the temperature rise of the hard drive above ambient by 21%, from 27.8 °C above ambient to 21.9 °C. The corresponding temperature rise of the left palm rest, directly above the hard drive, was reduced by 35% from 16.2 °C to 10.5 °C, while the rise in temperature of the right palm rest increased from 2.9 °C to 7.3 °C. All spreaders tested had a 13 μm thick PET film affixed to their surface to provide electrical insulation. CFD modeling indicates that contact resistance of the PET layers did not have a significant effect on the performance of the spreader in this application.

The net effect of the changes in touch temperatures was to reduce the temperature gradient between the left and right palm rests from

11.1 °C to only 2.9 °C. This reduction in case temperature gradient results in more comfortable operating conditions for the user.

REFERENCES

[1] Anschel, M., and Sammakia, B.G., 1990, "Electronic Package with Heat Spreader Member," US Patent No. 4914551.

[2] Mahulikar, D., Tyler, D.E., Braden, J.S., Pepplewell, J.M., 1997, "Molded Plastic Semiconductor Package Including Heat Spreader," US Patent No. 5608267.

[3] Chu, R.C., Ellsworth, M.J. Jr., Simons, R.E., 2002, "Thermal Spreader and Interface Assembly for Heat Generating Component of an Electronic Device," US Patent 6396700 B1.

[4] Jagannadham, K., 1998, "Multilayer Diamond Heat Spreaders for Electronic Power Devices," Solid State Electronics, Vol. 42, No. 12, pp. 2199-2208.

[5] Hall, D.R., Fox, J.R., 2002, "High-Pressure High-Temperature Polycrystalline Diamond Heat Spreader," US Patent Application Publication No. US2002/0023733 A1.

[6] Houle, S.J., Koning, P.A., Chrysler, G.M., 2002, "Carbon-Carbon and/or Metal-Carbon Fiber Composite Heat Spreaders," US Patent Application Publication No. US2002/0038704 A1.

[7] Kowbel, W., Patel, K., Champion, W., Withers, J.C., 2000, "Low Cost, High Thermal Conductivity Composites for Power Electronics," Proceedings, SAMPE 2000 Bridging the Centuries, 45th Conference, Long Beach, California, USA, May 21-25 2000.

[8] Watchko, G.R., Gagnon, M.T., Liu, P.W., deSorgo, M., Rodrtues, C.V., Lionetta, W.G., Oppenheim, S.M., 2003, "Thermal-Sprayed Metallic Conformal Coating used as Heat Spreaders," US Patent Application Publication No. US2002/0066672 A1.

[9] Weinstein, R.D., Hodes, M., Piccini, J.M., 2001, "Improved Static and Trasient Thermal Management of Handsets Using Heat Spreaders and Phase Change Materials (PCMS)," Proceedings, ASME NHTC'01, 35th National Heat Transfer Conference, Anaheim, California, USA, June 10-12, 2001.

[10] Dilley, R.L., Kiser, C.E., 2000, "Carbon/Carbon Heat Spreader," 2000, US Patent No. 6052280.

[11] Murthy, S., Joshi, Y., Nakayama, W., 2004, "Two-Phase Heat Spreaders Utilizing Microfabricated Boiling Enhancement Structures.", Heat Transfer Engineering, Vol. 25, No. 1, pp 26-36.

[12] Tzeng, J.W., Getz, G., Fedor, B.S., Krassowski, D.W., 2000, "Anistropic Graphite Heat Spreader for Electronics Thermal Management," Proceedings, International PCIM/Power Quality Conference, Nuremberg, Germany June 6, 2000.

[13] Ritchey, III, J.B., 2000, "Flexible Heat Transfer Device and Method," US Patent No. 6131651.

[14] Messenger, T.R., Whiting, I.M., 2001, "Heat Spreader," US Patent No. 6215661 B1.

[15] Kobayash, T., Ogushi, T., Sumi, N., Fujii, M., 1998, "Thermal Design of an Ultra-slim Notebook Computer," Proceedings, IEEE Intersociety Conference on thermal Phenomena, 1998.

[16] Kobayashi, T., Nonaka, T., 1999, "Heat Sink Assembly including Flexible Heat Spreader Sheet," US Patent No. 5991155.

[17] Dell USA Community Forum, 2005, "D600 Palmrest Heat," Online
(Available:
http://forums.us.dell.com/supportforums/board/message?board.id=latit_harddrive&message.id=6271)

[18] Jose Sandoval .com, 2005, "Hot Dell – D600 or D800 or whatever," Online
(Available: http://www.josesandoval.com/hotdells/)

[19] Vichare, N., Rodgers, P., Eveloy, V., Pecht, M.G., 2004, "In Situ Temperature Measurement of a Notebook Computer – A Case Study in Health and Usage Monitoring of Electronics," IEEE Transactions of Device and Materials Reliability, Vol. 4, No. 4, pp 658-663.

[20] Wagoner, G., Skokova, K.A., levan, C.D., 1999, "Angstrom's Method for Thermal Property Measurements of Carbon Fibers and Composites," Proceeding, Carbon '99, 24th Binnial Conference on Carbon, July 11-16 1999.

[21] American Society for Standard and Materials, "Standard Test Method for Determining Specific Heat Capacity by Differential Scanning Calorimetry," ASTM E 1269-05

[22] Anonymous, 2004, *The Industrial Graphite Engineering Handbook*, UCAR Carbon Company, Inc., A GrafTech International Ltd. Co. Clarksburg West Virginia, USA, pp.4-14 to 4-16.

[23] American Society for Standard and Materials, "Standard Test Methods for Thermal Transmission Properties of Thin Thermally Conductive Solid Electrical Insulation Materials," ASTM D 5470-95.

[24] Smalc, M., Norley, J., Reynolds, R.A. III, Pachuta, R., Krassowski, D.W., 2003, "Advanced Thermal Interface Materials using Natural Graphite," Proceedings, IPACK03, International Electronics Packaging Technical Conference and Exhibition, Maui, Hawaii, USA, July 6-11, 2003.

[25] Pollock, M., editor, 2002, *Grafoil Flexible Graphite Engineering Design Manual*, Second Edition, Graftech International Ltd., Cleveland, Ohio USA, p. 24.

[26] Anonymous, "Mylar[®] Polyester Film Product Information," DuPont Teijin Films, Wilmington, Delaware, USA

[27] American Society for Standard and Materials, "Standard Test Method for Resistance to Bending of Paper and Paperboard (Taber-Type Tester in Basic Configuration)," ASTM D 5342-97.